# Structural and biophysical properties of a synthetic channel-forming peptide: Designing a clinically relevant anion selective pore ☆

U. Bukovnik [a], J. Gao [a], G.A. Cook [a], L.P. Shank [a], M.B. Seabra [a], B.D. Schultz [b], T. Iwamoto [a], J. Chen [a], J.M. Tomich [a,*]

[a] Department of Biochemistry, Kansas State University, Manhattan, KS 66506, USA
[b] Department of Anatomy and Physiology, Kansas State University, Manhattan, Kansas 66506, Kansas State University, Manhattan, KS 66506, USA

## ARTICLE INFO

## ABSTRACT

The design, synthesis, modeling and *in vitro* testing of channel-forming peptides derived from the cys-loop superfamily of ligand-gated ion channels are part of an ongoing research focus. Over 300 different sequences have been prepared based on the M2 transmembrane segment of the spinal cord glycine receptor $\alpha$-subunit. A number of these sequences are water-soluble monomers that readily insert into biological membranes where they undergo supramolecular assembly, yielding channels with a range of selectivities and conductances. Selection of a sequence for further modifications to yield an optimal lead compound came down to a few key biophysical properties: low solution concentrations that yield channel activity, greater ensemble conductance, and enhanced ion selectivity. The sequence NK$_4$-M2GlyR T19R, S22W (KKKKPARVGL-GITTVLTMRTQW) addressed these criteria. The structure of this peptide has been analyzed by solution NMR as a monomer in detergent micelles, simulated as five-helix bundles in a membrane environment, modified by cysteine-scanning and studied for insertion efficiency in liposomes of selected lipid compositions. Taken together, these results define the structural and key biophysical properties of this sequence in a membrane. This model provides an initial scaffold from which rational substitutions can be proposed and tested to modulate anion selectivity. This article is part of a Special Issue entitled: Protein Folding in Membranes.

© 2011 Elsevier B.V. All rights reserved.

## 1. Introduction

Mutations in genes encoding ion channel proteins result in defective or absent channels, which are accompanied by the development of disease pathogeneses. One such channelopathy is cystic fibrosis (CF), the hereditary disease caused by mutations in the gene coding for the CF transmembrane conductance regulator (CFTR) [1]. Numerous cataloged mutations cause loss of function or poor cytosolic trafficking of the CFTR anion channel [1,2] and lead to epithelial electrolyte transport abnormalities [3,4] in several organ systems [2]. Ion-channel defects have been identified also in cation-selective channels, among which potassium channels are prevalent. A few examples include: persistent hyperinsulinemic hypoglycemia of infancy and Bartter's syndrome resulting from a loss-of-function of inwardly rectifying potassium channels [5] or neuromyotonia and episodic ataxia type 1 caused by dysfunctional voltage-sensitive potassium channels [6].

Symptomatic current treatment approaches for channelopathies focus on replacing or restoring function to defective ion channels or attenuating their negative phenotypic effects by employing mutation-specific pharmacotherapies [1], pharmacoagents alone [7,8] or a variety of genetic approaches. None of the available approaches is fully successful. An alternative to existing therapies could be the use of synthetic channel-forming peptides (CFPs), which would generate an ion-conducting pore with the appropriate CFP selectivity in appropriate tissues. CFPs can be *de novo* sequences [9,10] or based on segments of native proteins. The use of chemistry to design compounds corresponding to putative transmembrane regions of natural proteins yields detectable channel activities of CFPs in planar lipid bilayers [11–13] and human erythrocyte membranes [14]. Even though such constructs can be studied in greater detail than their parent proteins, CFPs are difficult to deliver from aqueous solution, lack the regulatory complexity of native proteins and exhibit reduced ion selectivity. However, since vectorial ion transport across epithelial tissues is accomplished with a constellation of contributing components, it is generally believed that some physiological regulation of complimentary proteins can modulate processes mediated by synthetic CFPs.

The glycine receptor (GlyR) was an obvious lead structure for developing an anion selective CFP because it is a ligand-gated anion channel [15] and a member of the cys-loop super family of ligand-gated channels [16]. GlyR is a heteropentameric oligomer [14,16] with four $\alpha$ subunits and one $\beta$ subunit [14]. The water-filled pores are

formed by the association of the second transmembrane segment (M2) contributed by each of the five subunits. An α-subunit homopentameric channel recapitulated physiological functions when expressed and evaluated in *Xenopus* oocytes [17]. This result suggested that an assembly of α-M2 sequences could generate a functional anion selective channel. Indeed, the native α-subunit M2 segment, PARVGLGITTVLTMTTQSSGSRA, forms chloride selective channels in lipid bilayers and single cells, and facilitates ion transport across epithelial monolayers [18,19]. The first sequence showed net transepithelial ion transport comparable to the parent M2GlyR channel pore [18], but poor efficiency with regard to membrane insertion and a tendency to form aggregates in aqueous solutions [18,19]. Subsequently, template-variants of the pore-lining M2 segment in a single peptide were prepared to evaluate the stoichiometry of the functional pore [12,18,20–23]. Results indicated that monomers assembled into pentameric structures where all of the peptides were inserted in the membrane with the same orientation. Preparing such large peptides, however, was too labor intensive and too expensive to be practical from a therapeutic standpoint. Studies were thus focused on preparing a monomer that would self-assemble into an anion selective pore.

Peptide sequences were modified by introducing multiple lysyl-residues at the N-termini to improve the solubility of the peptide and ensure the uniformity of orientation in the membrane [24]. Lysines at the termini of transmembrane sequences position themselves in the aqueous phase near the lipid phosphate groups [25] while their side chains direct electrostatic interactions with ions [26], the later could aid in anion selectivity. A tetralysyl tail on these peptides proved optimal, giving enhanced solubility without apparently altering channel properties [24]. Subsequently, the sequence was truncated by five residues at the C-terminus and the resulting C-terminal serine was replaced by tryptophan to reduce or eliminate solution aggregation [27–30]. As a result the peptide showed better efficiency of insertion into epithelial cell membranes [27], a decreased propensity for aggregation in aqueous solution [24,28] and increased transepithelial net ion transport at lower peptide concentrations when compared to the wild-type M2GlyR sequence [28]. Tryptophan and lysine play important roles in peptide orientation and in membrane insertion [25]. Tryptophan in proteins with transmembrane segments is known for its specific affinity for sites near the lipid carbonyl region [25]. A tryptophan containing sequence exhibited a decrease in the concentration required for net transepithelial ion conductance and an increase in the ability to adopt a helical secondary structure [29–31]. Furthermore, tryptophan and arginine reportedly play roles as anchors of transmembrane helices [32]. The threonine at position 19 was replaced with arginine to introduce a second anchor [30]. The resulting peptide showed increased net transepithelial ion conductance compared to the non-substituted wild type peptide. This sequence was also tested for antigenic activity in mice at proposed clinical dosages [33], and was negative. A descriptive name, NK$_4$-M2GlyR p22-T19R S22W, was given to this peptide: (KKKKPARVGL-GITTVLTMRTQW). The structural and biophysical characteristics of NK$_4$-M2GlyR p22-T19R S22W, a lead candidate peptide with potential as a therapeutic agent, are included in this report. The structure of a monomer was analyzed by circular dichroism (CD) and determined by solution nuclear magnetic resonance (NMR) in both trifluoroethanol (TFE) and sodium dodecylsulfate micelles (SDS). The outcomes indicated that a monomer of NK$_4$-M2GlyR p22-T19R S22W adopts a linear helical structure in hydrophobic environments. Structural models of the assembled pentameric channel were then constructed by incorporating additional experimental data and theoretical considerations. Subsequent 100–200 ns simulations of the channel structures in fully solvated lipid bilayers predicted the most probable handedness of helix assembly in the channel and suggested that the peptide was able to form well ordered pores in a membrane. A parallel set of experiments was conducted to identify the pore-lining residues

of assembled NK$_4$-M2GlyR p22-T19R S22W monomers by introducing selected cysteine modifications followed by channel blockade with thiol binding mercurial salts. While most sequences failed to insert into the synthetic bilayers, several sequences provided positional data on the location of pore-lining residues. Importantly, the identities of these pore-lining residues are fully consistent with those predicted by atomistic simulations. This suggests that the proposed structure of the pentameric channel formed by NK$_4$-M2GlyR p22-T19R S22W is realistic, thus providing a structural basis for understanding the channel activity and for devising rational strategies to design new sequences with improved functions. Efficiency of peptide insertion into artificial membranes was also evaluated, as the ability of synthetic peptides to interact with membranes depends not only on peptide's sequence [25] but also on the lipid composition of targeted membranes [25,34]. Lipids commonly present in bacterial and mammalian cell membranes were employed, as these surfaces will be encountered by CFPs when employed therapeutically. As detailed structure/function information on synthetic channels still remain largely unknown, the reported results add new information to the field of synthetic pore design.

## 2. Materials and methods

### 2.1. Peptide synthesis and purification

Peptides were synthesized using solid-phase peptide synthesis (Applied Biosystems Model 431A peptide synthesizer; Foster City, CA) employing 9-fluorenylmethoxycarbonyl (Fmoc) chemistries [24,35,36]. CLEAR amide resin, (0.3 mmol/g; Peptides International, Louisville, KY) and N$^\alpha$-Fmoc amino acids (Anaspec Inc., San Jose, CA) were used. All peptides were HPLC (System Gold HPLC; Beckman Instruments, Inc., Fullerton, CA) purified using a reversed-phase C-18 column (Phenomenex, Torrance, CA) and eluted from the column using a linear gradient of 3.0% min$^{-1}$ of 10–90% acetonitrile containing 0.1% trifluoroacetic acid (TFA) at 1 mL/min [37]. HPLC-purified peptides were characterized by matrix-assisted-laser desorption time-of-flight mass spectroscopy (MALDI-TOF/TOF; Bruker Ultraflex III, Bruker Daltronics, Billerica MA). After characterization, peptides were lyophilized and stored as dry powders until used. All peptide concentrations were determined by measuring the absorbance at 278 nm, and using the tryptophan extinction coefficient (ε) of 5579 M$^{-1}$ cm$^{-1}$ at 278 nm.

### 2.2. CD

CD (spectropolarimeter models J-720 or J-815, Jasco, Tokyo, Japan) was employed to determine the secondary structures of peptides dissolved in water, TFE and SDS using conditions described previously [29]. Peptide concentrations ranging from 20 μM to 3 mM were tested depending on the experiment.

### 2.3. Solution NMR spectroscopy

Lyophilized peptide was dissolved in a (1:1) mixture of 1,1,1,3,3,3-Hexafluoro-2-propanol/2,2,2-Trifluoroethanol at 3 mM. This solution was added to SDS dissolved in deionized/distilled (DD) H$_2$O at a ratio of peptide to SDS of 1:150. The mixture was vortexed and an excess amount of deionized distilled (DD) H$_2$O was added to equal 16 times the volume of TFE. The later step ensured that the peptide inserted into the micelles. The sample was lyophilized overnight and then the NMR sample prepared by dissolving the dry powder in 90% H$_2$O and 10% D$_2$O. Use of different solvents for the NMR sample preparation showed that SDS micelles are optimal for stabilizing the peptide's structure thereby yielding better NOE constraints.

Spectra of the NK$_4$-M2GlyR p22-T19R, S22W peptide were recorded at 40 °C (Bruker Avance-800 NMR spectrometer, Bruker

Instruments, Billerica, MA) equipped with a triple resonance probe. The duration of the 90° pulse was ~9 μs for 1H. Two-dimensional NOESY and TOCSY data were acquired in phase-sensitive (States-TPPI) mode into 2048 t2 and 256 t1 points with spectral width of 10 ppm in each dimension, and 72–80 transients per increment. A spinlock time of 100 ms was used for TOCSY and mixing times of 100 and 200 ms for NOESY were used. For suppression of the solvent peak, the WATERGATE pulse scheme was applied in the TOCSY experiment and water flipback was used for the NOESY experiment. Data from both sets of experiments were processed using NMR Pipe [38] and analyzed using Sparky software [39]. NMR structure calculations were prepared as described previously [29].

## 2.4. Molecular modeling and simulation protocols

Three models of the putative pentameric pore were constructed with three different handedness orientations of helix packing: left-handed, straight and right-handed, using a strategy similar to previous work [31]. The pentameric structures were solvated in pre-equilibrated POPC bilayers using the CHARMM-GUI automated Membrane Builder [40,41]. The final systems consisted of ~100 lipids, ~4800 water molecules, ~10 $K^+$ and ~40 $Cl^-$, besides the proteins. The box size was ~$65 \times 65 \times 72$ Å. A protocol similar to one used in previous work [31] was applied to equilibrate the system at 303 K using CHARMM [42,43], during which various restraints were applied to selected heavy atoms with gradually decreasing restraint strength. SHAKE was used to fix the length of hydrogen-attaching bonds [44], particle mesh Ewald (PME) [45] was used for long-range electrostatic interactions, and van der Waals interactions were smoothly switched off from 10 to 12 Å. The equilibrated structures were then used to initiate production simulations using NAMD [46]. Another 100 ps equilibration simulation with weak harmonic positional restraints on protein backbone atoms ($k = 0.1$ kcal/mol/Å$^2$) was used to suppress potential strains during subtle differences between CHARMM and NAMD. Setups equivalent or identical to those used in CHARMM equilibration simulations were used in NAMD runs. The length of production simulation was 100 ns for left-handed and straight pore assemblies, and extended to 200 ns for the right-handed model to probe the preferred handedness of the pore assembly further. These simulations are much longer than those published previously for NK$_4$-M2GlyR p22 and NK$_4$-M2GlyR p22-S22W pores [31]. The purpose of longer simulations is to better exploit the force field to resolve the handedness of pore assembly, a key feature that has not been determined experimentally. The coordinates were saved every 1 ps for post-analysis. All analyses were performed using CHARMM. VMD [47] was used for visualization and preparation of molecular images for presentation. The pore profiles and estimated ion conductances were calculated using the program HOLE with default options [48].

## 2.5. Identification of pore-lining residues

### 2.5.1. Cysteine scanning study
Seventeen cysteine substituted variants of NK$_4$-M2GlyR p22-T19R, S22W were synthesized. The following replacements were synthesized as described above: K3C, K4C, P5C, A6C, V8C G9C, L10C, G11C, I12C, T13C, T14C, V15C, L16C, T17C M18C, T20C and Q21C. Three peptide concentrations (60, 100, and 200 μM) were employed to assess effects on short-circuit current ($I_{SC}$), a sensitive indicator of net active ion transport across epithelial monolayers, as described below.

### 2.5.2. Trans epithelial ion transport measurements
Madin-Darby canine kidney (MDCK) epithelial cells were a generous gift of Dr. Lawrence Sullivan (KUMC, Kansas City, KS). The cells were cultured as described previously [19]. 1-ethyl-2-benzimidazolinone (1-EBIO; Acros, Morris Plains, NJ) was prepared as a 1 M stock solution in dimethyl sulfoxide (DMSO).

Transepithelial ion transport was evaluated employing modified Ussing chambers (Model DCV9, Navicyte, San Diego, CA). MDCK cell monolayers were mounted vertically in chambers. Apical and basolateral aspects of the monolayers were bathed in a modified Ringer solution (in mM; 120 NaCl, 25 NaHCO$_3$, 3.3 KH$_2$PO$_4$, 0.8 K$_2$HPO$_4$, 1.2 MgCl$_2$, and 1.2 CaCl$_2$), which was prepared fresh daily and all components were purchased from Sigma-Aldrich (St. Louis, MO). The bathing solution was kept at 37 °C and continuously bubbled with 5% CO$_2$/95% O$_2$ to maintain pH, provide aeration and mix fluid in chambers. Experiments were conducted on monolayers with a resistance of at least 600 Ω cm$^2$. The transepithelial membrane potential ($V_{TE}$) was clamped to 0 mV and the $I_{SC}$ measured continuously with a voltage clamp apparatus (Model 558C, University of Iowa, Department of Bioengineering, Iowa City, IA). Data acquisition was performed at 1 Hz with an Intel-based computer running AcqKnowledge software (version 3.7.3, BIOPAC Systems, Santa Barbara, CA) with an MP100A-CE interface. The data points represent the mean $I_{SC}$ stimulated by the peptides at the indicated concentrations. Bars indicate the standard error of the mean. The differences between the control and treatment data were analyzed using ANOVA and Student's t-test. The probability of making a type I error less than 0.05 was considered statistically significant. The lines presented in some figures represent the best fit of a modified Hill equation to the data, $I_{SC} = I_{MAX} * (x^n/(K^n_{1/2} + x^n))$; where K$_{1/2}$ is the concentration of peptide that provides a half maximal $I_{SC}$ and n represents the Hill coefficient.

## 2.6. Interaction of NK$_4$-M2GlyR p22-T19R, S22W with large unilamellar vesicles

All phospholipids were purchased from Avanti Polar-Lipids, Inc., (Alabaster AL). Stock solutions of POPC: (1-Palmitoyl-2-oleoyl-sn-glycero-3-phosphocholine), POPG:(1-Palmitoyl-2-oleoyl-sn-glycero-3- phospho-rac-(1-glycerol)), POPS: (1-Palmitoyl-2-oleoyl-sn-glycero-3-phospho-L-serine), POPE: (1-Palmitoyl-2-oleoyl-sn-glycero-3-phosphoethanolamine), DLPC: (1,2-Dilauryl-sn-glycero-3 -phosphocholine) and DLPG: (1,2-Dilauryl-sn-glycero-3-phospho-rac-(1-glycerol)) stored in chloroform were used and mixed by volume to obtain the appropriate molar ratios of negatively charged phospholipids. The chloroform was evaporated under a stream of nitrogen gas. Lipid mixtures were resuspended in deionized water at room temperature to yield a total lipid concentration of 10 mM. Suspensions were incubated at 40 °C for an hour with frequent vigorous agitation and then passed through polycarbonate membrane (100 nm pore size; Avanti Mini extrude, Avanti Polar-Lipids, Inc.) to prepare large unilamellar vesicles (LUVs). One milliliter of LUV suspension was placed into a cleaned vial and 1 mL of peptide (10 μM) was added, giving final concentrations of lipid and peptide of 1 mM and 5 μM, respectively.

## 2.7. Fluorescence spectroscopy

Fluorescence spectroscopy was employed for blue shift analyses in the emission spectra for peptides inserted into micelles with different lipid combinations. Fluorescence spectra were recorded (Hitachi F-4010 or Cary Eclipse fluorescence spectrophotometer) with an excitation slit width of 3–5 nm and emission slit width of 5 nm. The excitation wavelength was set at 278–280 nm and the emission spectra recorded from 300 to 500 nm. All measurements were made in a $10 \times 10$ mm cuvette at 25 °C. For samples containing vesicles, the background was subtracted from the peptide-containing samples. A final peptide concentration of 5.0 μM in deionized water or in 1 mM freshly prepared large unilamellar vesicles (LUVs) of either POPC: POPG (7:3) or DLPC:DLPG (7:3) was used. This protocol was adapted from that described previously [49].

Peptide and liposome solutions were incubated one hour prior to recording the spectra. Values recorded from a sample containing only liposomes were subtracted from the samples containing the vesicles and peptide. All the measurements were performed in triplicate. The lipid: peptide molar ratio was kept at 200:1 throughout all experiments.

## 3. Results and discussion

The peptide NK$_4$-M2GlyR p22-T19R, S22W represents the best candidate for additional modifications and/or potential therapeutic use. Substitutions made to the parent NK$_4$-M2GlyR p27 sequence (Table 1) yielded a peptide with many desirable properties that relate to solubility, aggregation, immune and inflammatory responses and ion permeation. In producing this well-behaved sequence, anion selectivity was negatively impacted. The parent NK$_4$-M2GlyR p27 sequence had permeation selectivities greater than 25:1 for monovalent anions over monovalent cations [24]. This value in NK$_4$-M2GlyR p22-T19R, S22W is now 1.4:1 [30]. Before planning additional substitutions to remedy this shortcoming, the structure of this peptide had to be determined to identify pore-lining residues. During these studies it was observed that lysine containing sequences produced robust current generating responses in epithelial mono-layers and oocytes but not in synthetic bilayers. Therefore the insertion efficiency into synthetic membranes with different binary lipid compositions was analyzed to begin to understand this phenomenon.

### 3.1. Overall secondary structure characteristics

Employing CD, the mean molar ellipticity spectrum for NK$_4$-M2GlyR p22-T19R, S22W (50 μM) was generated and compared to those recorded for three earlier designs: NK$_4$-M2GlyR p22, NK$_4$-M2GlyR p27-WT and NK$_4$-M2GlyR p22-S22W (Table 1). The spectrum of NK$_4$-M2GlyR p22-T19R, S22W indicated helical content with characteristic α-helix double minima at 208 and 222 nm and a maximum at ~192 nm. Similar characteristics were obtained for other related peptides, as shown with overlaid spectra (Fig. 1). Results are in agreement with secondary helical structures determined in previous studies with these earlier sequences [29,30]. The spectra indicate that the replacement of the threonine at position 19 with the cationic arginine residue does not affect the propensity to adopt a helical conformation in a hydrophobic environment.

Prior to collecting any NMR spectra, the effect of peptide concentration on secondary structure and aggregation in SDS were assessed as a function of time. The peptide was analyzed at two concentrations, 50 μM and 3.0 mM, which was used also for the NMR experiments. Spectra were obtained in a 200-fold molar ratio of detergent monomer to peptide for the SDS micelles (10 mM and 600 mM, respectively) at various temperatures. Under these condi-tions there should be, on average, just one peptide per micelle. When corrected for peptide concentration the results obtained at the two concentrations were indistinguishable and indicated that the peptide did not aggregate at the concentration and temperatures used for NMR (data not shown). Samples that were stored at room temperature showed no discernable change in their CD spectra when re-examined over a two-week period.
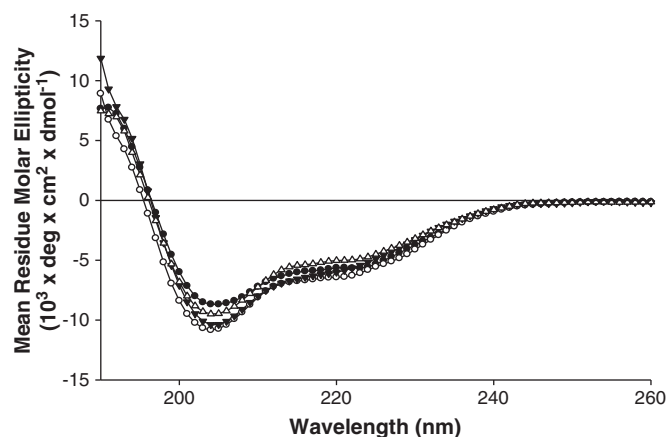


**Fig. 1.** Circular dichroism spectra of NK$_4$-M2GlyR derived peptides in 10 mM SDS micelles. Spectra represented include peptides: NK$_4$-M2GlyR p27 WT (●), NK$_4$-M2GlyR p22 (○), NK$_4$-M2GlyR p22-S22W (▼), and NK$_4$-M2GlyR p22-T19R, S22W (△) with peptide concentrations of 50 μM. Spectra were recorded at ambient temperature (22 °C) and represent averages of eight scans after subtraction of the reference spectra of the media.

### 3.2. Solution nuclear magnetic resonance (NMR)

The different NMR spectra of NK$_4$-M2GlyR p22-T19R, S22W were recorded in deuterated SDS. Under the conditions employed, the structure generated is of the monomer encapsulated within a C$_{12}$ acyl chain detergent micelle. All spectra were indistinguishable from those used to generate the solution NMR structure for NK$_4$-M2GlyR p22-S22W [31]. The new results show that residues 10–20 of NK$_4$-M2GlyR p22-T19R, S22W have resonances expected for helical conformation, while the N-terminus is largely disordered. Overlaying the NOESY spectrum for NK$_4$-M2GlyR p22-T19R, S22W with that of NK$_4$-M2GlyR p22-S22W shows significant similarities and several important differences (Fig. 2, Table 2). The two-dimensional $^1$H–$^1$H NOESY analysis provided 150 distance constraints, 52 of which were inter-residue constraints (sequential, medium and long range). A number of long-range NOE connectivities typical for α-helical conformation were observed. In 2D $^1$H–$^1$H NOESY spectra, dαβ (i, i+3) connec-tivities were identified for G11-T14, I12-V15, V15-M18 and L16-R19. Six dihedral angle constraints were calculated from $^3$J coupling constants. The target function for the structure was 0.30 ± 0.12 . NOE constraint violations were limited and the sum of the violations was 1.68 ± 0.50 . 1 dihedral angle violation of 0.25° was observed. Ramachandran values showed that the backbone torsional angles were all within allowed regions.

Table 2 shows data obtained for this peptide. Structural statistics include the RMSD value for the structures within the cluster from the mean structure with lower values obtained for NK$_4$-M2GlyR p22-T19R, S22W compared to values previously published for NK$_4$-M2GlyR p22-S22W [29]. Representative conformation models for solution structures of both peptides are shown in Fig. 3. The peptides adopt slightly different conformations. NK$_4$-M2GlyR p22-S22W appears to have a more curved structure while NK$_4$-M2GlyR p22-T19R, S22W adopts a more linear conformation. These sequences were subsequently analyzed as five-helix assemblies using MD simulations.

### 3.3. Structural characterization of the channel assembly

#### 3.3.1. Stability of the channel structures in POPC bilayers

Three models of the putative pentameric pore of NK$_4$-M2GlyR p22-T19R, S22W (Fig. 4) were constructed with different handedness of helix packing: left-handed, straight and right-handed, respectively. Similar to previous work with NK$_4$-M2GlyR p22-S22W (31), the tilt angle of the initial left-handed and right-handed models is 15°. The
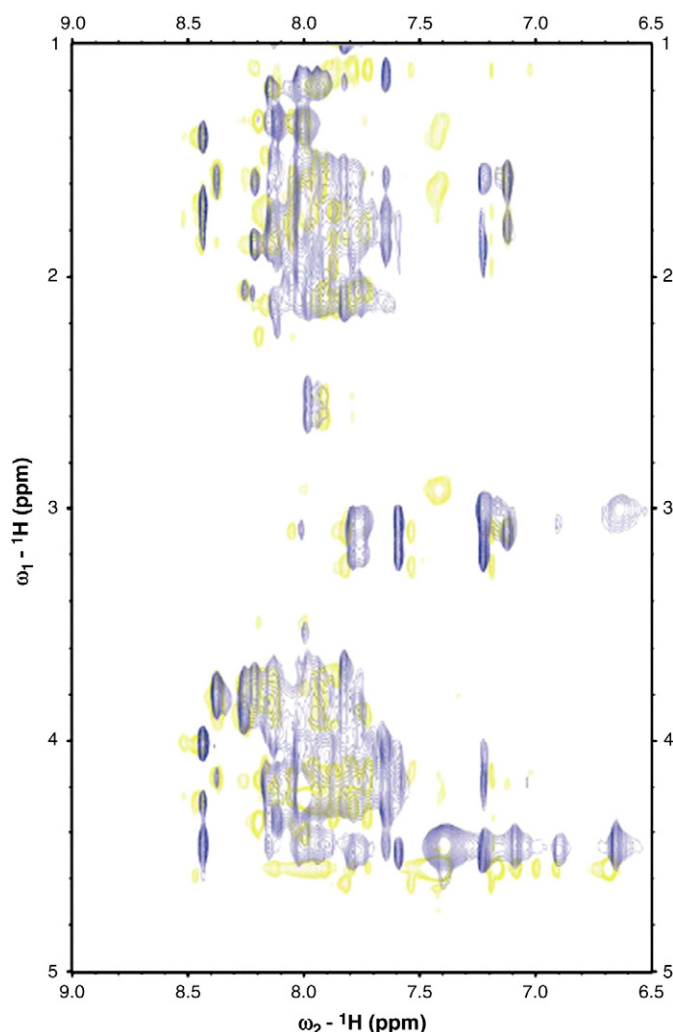
**Table 1**
Sequences of NK$_4$-M2GlyR derived peptides.

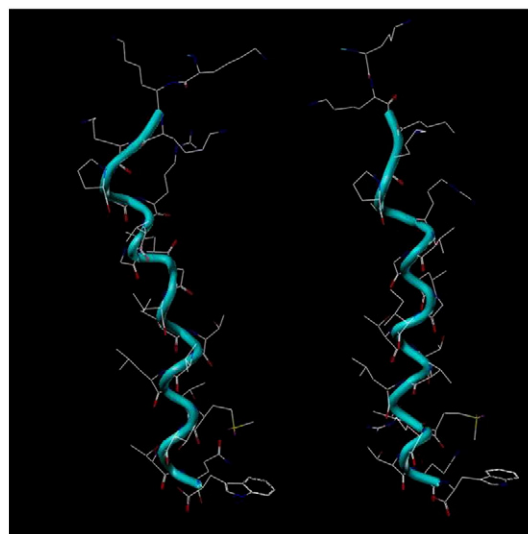| Protein ID [ref] | Sequence | Mol. wt. (Da) |
|---|---|---|
| NK$_4$-M2GlyR p27 WT [19] | KKKKPARVGLGITTVLTMTTQSSGSRA | 2817.4 |
| NK$_4$-M2GlyR p22 [28] | KKKKPARVGLGITTVLTMTTQS | 2358.9 |
| NK$_4$-M2GlyR p22-S22W [29] | KKKKPARVGLGITTVLTMTTQ**W** | 2458.0 |
| NK$_4$-M2GlyR p22-T19R, S22W [30] | KKKKPARVGLGITTVLTM**R**TQ**W** | 2512.1 |

**Fig. 3.** Calculated structure models of p22-S22W (left) and p22-T19R S22W (right) in SDS micelles. A representative conformation was modeled for the solution structures. The backbones are shown as a tube with the heavy atoms of the side chains visible in a wire frame.

initial pore-lining face was based on a consideration of the peptide's amphipathicity.

All three constructed structural models (Fig. S1), are stable throughout the production simulations. The ranges of RMSD values of the pore assembly as well as individual monomers from the initial models are similar to those for NK4-M2GlyR p22 and NK4-M2GlyR p22-S22W pores [31]. The moderate RMSD values are due mainly to the unstructured N-terminal lysines and flexibility in the channel assembly itself. Figs. 5 and S2 depict the evolution of the positions of the centers of the mass and two termini along membrane normal during the production simulations. Interestingly, NK4-M2GlyR p22-T19R, S22W channels appear to show substantial fluctuation along the membrane normal similar to NK4-M2GlyR p22 channels [31]. This suggests that T19R mutation could attenuate the membrane anchoring effects of NK4-M2GlyR p22-S22W. Importantly, the secondary structures and overall features of the pore assemblies (such as helix–helix packing interfaces and pore-lining residues analyzed below) are well conserved. For example, as shown in Fig. S3, the overall helicity stabilizes at ~70%, similar to the values observed for NK4-M2GlyR p22 and NK4-M2GlyR p22-S22W pores [31]. General conservation of the secondary and tertiary fold across all three sequences (NK4-M2GlyR p22, NK4-M2GlyR p22-S22W, and NK4-M2GlyR p22-T19R, S22W) is not surprising, as all these sequences have been shown to be capable to insert and form active channels, albeit with different levels of ion conductance.

### 3.3.2. Handedness of helical assembly

One of the unresolved structural features of the putative pores formed by M2GlyR-derived peptides is the most probable handedness of the helical assembly. Even though all available crystal structures of cys-loop ligand-gated ion channels contain left-handed packing of pore-forming transmembrane helices [50–53]. Previous simulations of limited length (20 ns) of NK4-M2GlyR p22 and NK4-M2GlyR p22-S22W channels were not able to identify any apparent difference between right- and left-handed assemblies [31]. One of the key objectives of the current simulations was thus to resolve this issue. Three models of the putative pentameric pore of NK4-M2GlyR p22-T19R, S22W (Fig. 4) were constructed with different handedness of helix packing: left-handed, straight and right-handed, respectively. Similar to our previous work on NK4-M2GlyR p22-S22W [31], the tilt angle of the initial left-handed and right-handed models is 15°. The
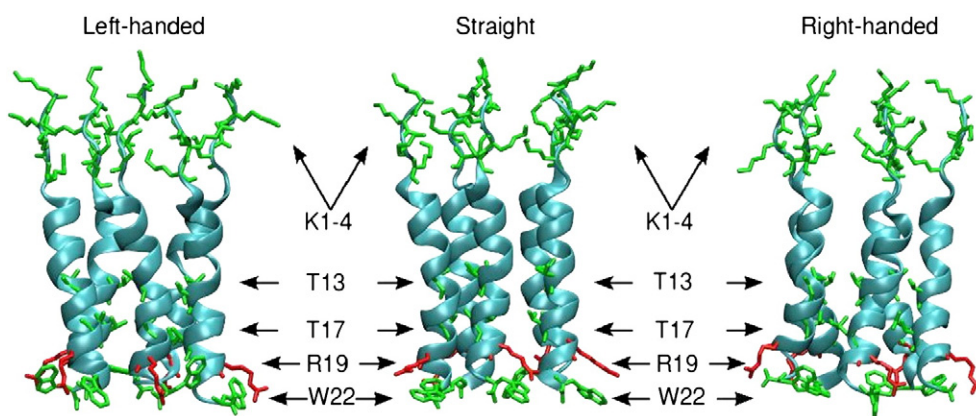
**Fig. 2.** Overlay of the NOESY spectra of NK4-M2GlyR p22-S22W (yellow) and NK4-M2GlyR p22- T19R, S22W (blue).

**Table 2**
Structure statistics of NK4-M2GlyR p22-T19R, S22W in SDS micelles.

| | NK4-M2GlyR p22-T19R, S22W |
|---|---|
| Target function (Å) | $0.30 \pm 0.12$ |
| Experimental NMR constraints | |
| NOE distance constraints | |
| Intraresidue | 98 |
| Sequential | 30 |
| Medium range | 15 |
| Long range | 7 |
| Angle constraints | 6 |
| NMR constraint violations | |
| NOE constraint violations (Å) | |
| Sum | $1.68 \pm 0.50$ |
| Maximum | $0.44 \pm 0.24$ |
| Angle constraint violations | |
| Sum | 0.00 |
| Maximum | 0.00 |
| Energy (kcal/mol$^{-1}$) | |
| $E_{total}$ | $-15.24 \pm 5.34$ |
| RMSD from the mean structure (Å) | |
| Residues 9–20 backbone atoms | $0.25 \pm 0.10$ |
| Ramachandran statistics | |
| Residues in allowed regions | >99% |
| Residues in generously allowed regions | <0% |
| Residues in disallowed regions | <0% |

**Fig. 4.** Initial 3D structural models of the pentameric channels. Side chains of key pore-lining residues (T13 and T17), the N-terminal lysines (K1-4), and membrane anchoring arginines and tryptophans (R19 and W22) are highlighted.

initial pore-lining face suggested was based on a consideration of the peptide's amphipathicity.

As shown in Fig. 6 and 7, the straight assembly drifted gradually towards left-handedness over the course of 100 ns production simulation, and adopted stable packing with a twist angle similar to the equilibrium value reached by the simulation of the left-handed assembly. The right-handed channel also appeared to drift toward left-handedness and became largely straight by the end of the first 100 ns production simulation. Therefore, simulation of the right-handed assembly was extended for another 100 ns, during which the channel indeed managed to switch the handedness around 160 ns. The final state at the end of the 200 ns production simulation is a left-handed assembly on average. However, the average twist angle (~8°) is significantly lower than the equilibrium values reached by simulations of the straight and left-handed assemblies (~20°), as shown in Fig. 6 and Supplement Materials (Fig. S4). The lower average twist angle is due to the heterogeneity in the assembly: only four of the five individual helix-helix packing interfaces switched to left-handed packing at the end of 200 ns simulation. It can be expected that the channel will eventually become fully left-handed with longer simulations. Therefore, longer production simulations reported here seem to resolve the handedness of the putative channels formed by M2GlyR-derived peptides and predict that these synthetic channels most likely have the same left-handed pore assembly as observed in the crystal structures of the full length channels [51].
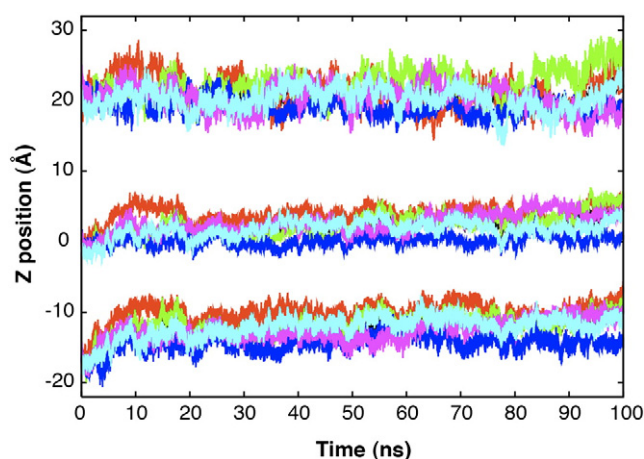
### 3.3.3. Helix packing, membrane-exposed and pore-lining residues

Details of helix packing and residue distribution of the pore were analyzed. The initial focus was on the left-handed assembly (Section 3.3.1.) that has been predicted to be the native state. Results summarized in Fig. 8a demonstrate that the pore is mainly lined with A6, R7, L10, T13, T14, T17, T20 and Q21. Note the N- and C-terminal residues, K1-4 and W22, should not be considered as pore-lining, even though they are indicated to have high pore-lining probabilities based on their contacts with (bulk) water molecules. The predicted pore-lining interface is largely consistent with the one derived from consideration of amphipathicity. However, the predicted pore-lining interface is broader due to substantial fluctuations of the pore. Participation of residues in helix–helix packing is characterized by calculating the average burial areas of side-chains, shown in Fig. 9b. Clearly, most residues with the structured region contribute to helix–helix interactions, except G9, G11, I12, V15 and R19. These residues either lack side chains (G9 and G11) or are fully membrane exposed. (I12, V15, L16 and R19). L10 and Q21 appear to be particularly important for stabilization of the pore assembly with largest buried surface areas (Fig. 8b).

### 3.3.4. Pore profiles

Average pore profiles calculated from the production simulations are shown in Fig. 9. The profiles derived from simulations of left-handed and straight assemblies are similar, consistent with the observation that the straight assembly evolved completely to a left-
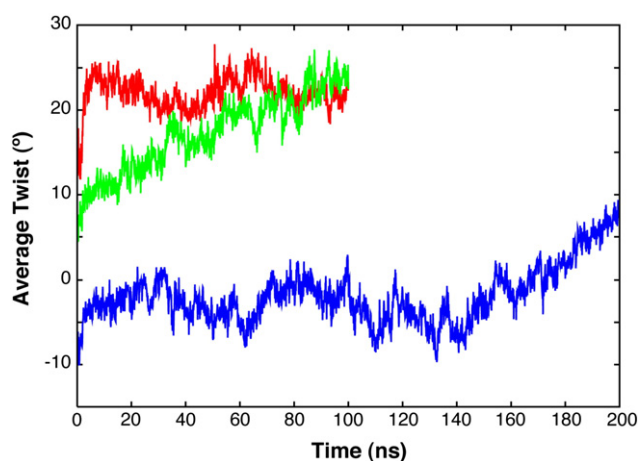


**Fig. 5.** The centers of mass and N-/C-terminal positions of whole protein and individual monomers of the left-handed channels along the membrane normal with respect to the lipid center of mass as functions of time. The N- and C-termini are represented by $C_\alpha$ atoms of K1 and W22, respectively. The monomer center of mass was computed using all heavy atoms. The black traces are for whole protein, and chromatic traces for individual monomers.



**Fig. 6.** Evolution of the handiness of helix packing as function of time for left-handed (red), straight (green) and right-handed assemblies (blue). The handiness is described by a virtual dihedral angle defined by two pairs of $C_\alpha$ atoms on two adjacent helices, $C_{\alpha,\ Leu10}$–$C_{\alpha,\ Trp22}$–$C'_{\alpha,\ Trp22}$–$C'_{\alpha,\ Leu10}$. The values shown are the averages of five helix–helix twist angles in the pentameric assembly.
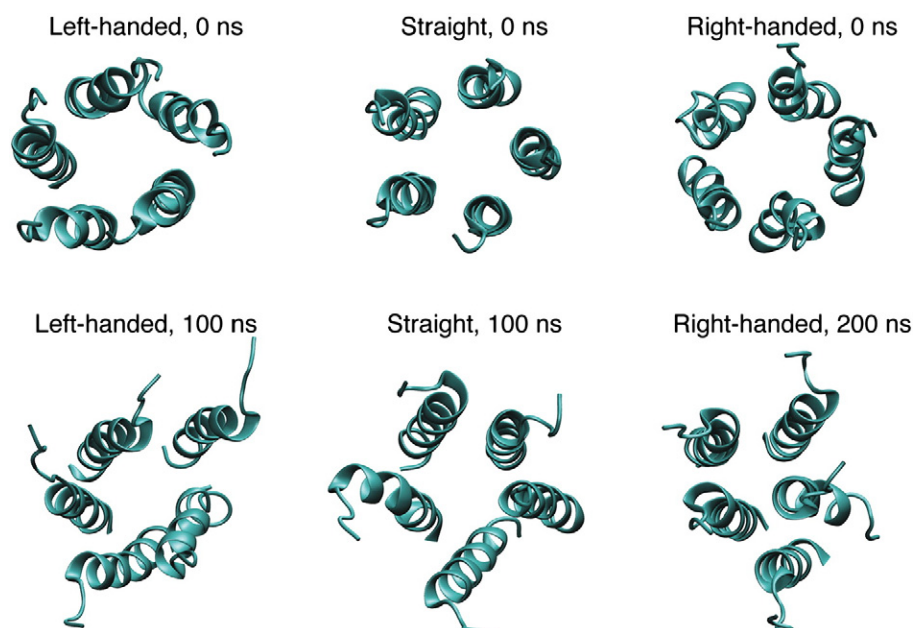
**Fig. 7.** The initial and final snapshots of the simulations of left-handed, straight and right-handed assemblies of p22-T19R/S22W.

handed one (see above). The pore profile derived from the simulation of the right-handed channel is slightly different from the other two, apparently due to a lack of convergence within 100 ns. Nonetheless, all three assemblies have similar radii at the narrowest region (near Thr17). Curiously, the p22-T19R, S22W pore appears to be slightly narrower than both p22 and p22-S22W pores [31]. This does not appear to be consistent with increased conductance measured using MDCK monolayers. It is not clear that this is an artifact of much longer simulations used in the current work compared to the previous work. Further free energy calculations using similarly refined structural models, together with new single channel measurements, will help to further clarify whether the atomistic modeling is able to recapitulate the expected difference in channel activity.

### 3.4. Cysteine scanning

Seventeen individual peptides with single cysteine substitutions at indicated positions in NK$_4$-M2GlyR p22-T19R, S22W (Table 6) were tested for their ability to induce ion secretion across the MDCK monolayers (Fig. 10) and identify any possible non-permissible substitution sites. The N-terminal lysines at positions 1 and 2, the arginines at positions 7 and 19 and tryptophan at the C-terminus were not substituted due to their involvement in insertion orientation, ion selectivity or membrane anchoring functions. The shaded gray bars in the figure represent the $I_{SC} \pm$ S.E.M. range for the parent NK$_4$-M2GlyR p22-T19R, S22W peptide at 60, 100, and 200 μM concentrations (bottom to top). The same three concentrations were used for each of
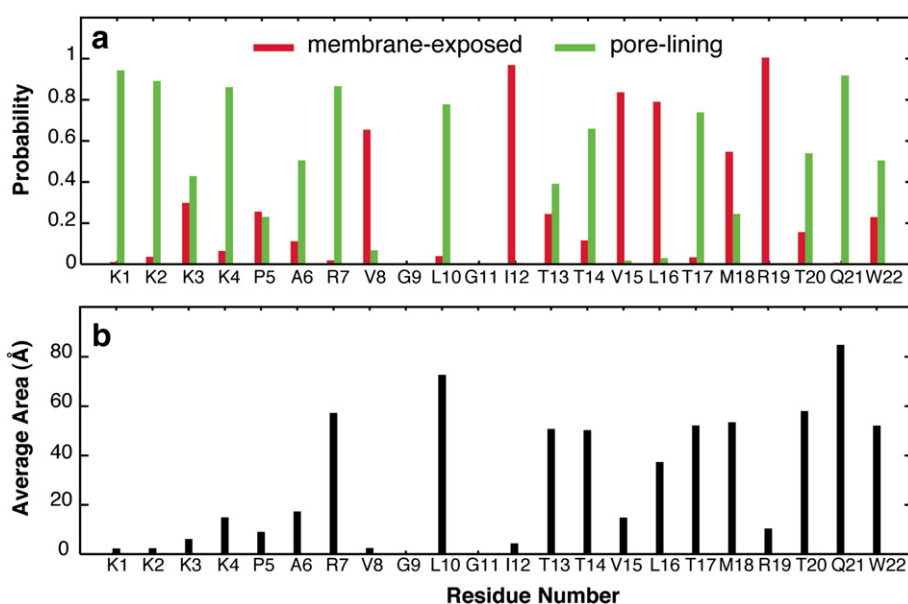


**Fig. 8.** a. Probabilities of a residue being either a pore-lining one or a membrane-exposed one. b. Average surface area of burial due to peptide–peptide interactions. The results are calculated from the last 80 ns of 100 ns production simulation of the left-handed channel.
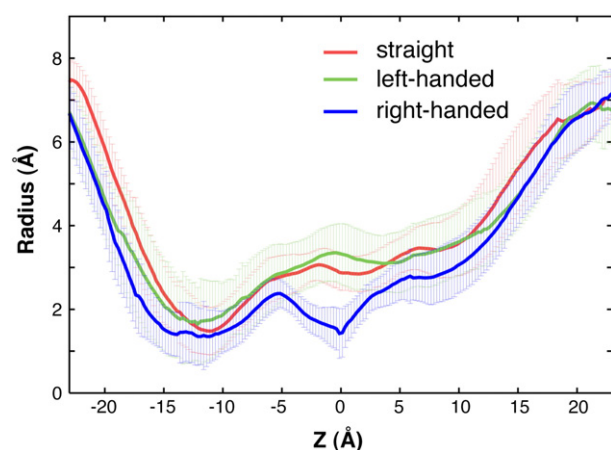
**Fig. 9.** Pore profiles with standard error bars along the channel principal axis. The averaged profiles were computed from snapshots taken very 1.0 ns from 20 to 100 ns production simulations. The snapshot pore profiles were calculated using the program HOLE [48]. The C-terminus is on the left and N-terminus on the right.

**Table 4**
Large unilamellar vesicles (LUVs) made by extrusion with POPC:POPS at different ratios (Error ± 1 nm). L/P ratio is 200/1.

| POPC (mol%) | POPS (mol%) | $\lambda_{max}$ (nm) |
|---|---|---|
| 0 | 0 | 356 |
| 100 | 0 | 356 |
| 90 | 10 | 342 |
| 80 | 20 | 339 |
| 70 | 30 | 335 |
| 60 | 40 | 338 |
| 50 | 50 | 339 |

based on refined NMR monomer structure showing the potential involvement of T13 in structural modifications of the pore. The narrowing of the pore observed in NK4-M2GlyR p22-S22W, which was absent in NK4-M2GlyR p22-T19R, S22W indicates that the position of the ring of OH groups contributed by Thr13 in NK4-M2GlyR p22-T19R, S22W have likely become repositioned thereby widening the pore and explaining the increased conductance observed.

### 3.5. Blockade experiments in artificial bilayers

The cysteine substituted peptide variants of NK4-M2GlyR p22-T19R, S22W were tested using synthetic bilayers in hopes of identifying the pore lining residues through channel blockade upon the addition of a mercurial salt. These experiments were, for the most part, unsuccessful. High resistance bilayers (70:30 POPC:POPS from decane) were formed at 100 mV, bathed in a symmetrical 0.1 M KCl, and allowed to stabilize before adding peptide (1–10 nM). Numerous attempts had to be made before obtaining just a few suitable channels for the following peptides (1) NK4-M2GlyR p22-T14C, T19R, S22W, (2) NK4-M2GlyR p22-V15C, T19R, S22W and (3) NK4-M2GlyR p22-V15C, T19R, S22W. No other sequences yielded recordable channels. For the three peptides where channel activity commenced, increasing concentrations of HgCl2 were added and the decrease in channel activity recorded. Based on the low concentration of HgCl2 required to inhibit channel activity for the T17C substitution, position 17 appears to be present in the pore of the channel. Based on the intermediate concentration of HgCl2 required to inhibit channel activity for the T14C substitution, this residue may be near or part of a helix-helix interface. Based on the high concentration of HgCl2 that fails to inhibit channel activity for the V157C substitution, this residue appears to face the lipids in the membrane. The results obtained for the three residues that produced pores are consistent with the modeling studies presented above.

### 3.6. Interaction of NK4-M2GlyR p22-T19R, S22W with LUVs of a series of POPC:POPS, POPC:POPE and POPC:POPG composition

Most of the tested sequences failed to show any channel activity in the bilayer assay. The fact that these sequences generate measurable

**Table 5**
Large unilamellar vesicles made by extrusion of POPC:POPG at different ratios (Error ± 1 nm). L/P ratio was 200/1.

| POPC (mol%) | POPG (mol%) | $\lambda_{max}$ (nm) |
|---|---|---|
| 0 | 0 | 352 |
| 100 | 0 | 353 |
| 90 | 10 | 351 |
| 80 | 20 | 345 |
| 70 | 30 | 342 |
| 60 | 40 | 344 |
| 50 | 50 | 345 |

the test sequences and are represented, for clarity, as slightly offset bars (laterally) that show the measured $I_{SC}$ ± S.E.M. values. They are plotted above the corresponding amino acid replaced by the cysteine. Net transepithelial ion transport rates showed that the replacements at the more terminal sites, K3, K4, P5, A6 or T17, M18, T20 and Q21 yielded transport rates higher at each concentration than that observed for the parent NK4-M2GlyR p22-T19R, S22W. Replacements in the central membrane embedded region generally led to lower flux values relative to NK4-M2GlyR p22-T19R, S22W except for the pore contributing Leu10, which yielded results nearly identical to the parent sequence. The lowest activities were observed for the cysteine substitutions at positions G9, G11, I12, V15 and L16. As discussed earlier these residues are most likely facing lipid and posses either no side chain or extended hydrophobic side chains. Introduction of a short hydrophilic side chain in these positions could affect membrane insertion or helix–helix packing.

The results are partially supported by the computer modeling assignments of the pore lining residues consisting of T13 and T17. Placing cysteine at position 17 resulted in an increase in $I_{SC}$ while the cysteine at position 13 showed a decrease in $I_{SC}$ compared to NK4-M2GlyR p22-T19R, S22W. This is an indication that T13 might not be a part of pore-lining surface, but could play a role in structural properties of assembled pore. This is in agreement with calculations

**Table 3**
Sequences of Cysteine scanning substituted peptides.

| | |
|---|---|
| 1. NK4-M2GlyR p22 T19R S22W | KKKKPARVGLGITTVLTMRTQW |
| 2. NK-K3C-M2GlyR p22 T19R S22W | KKCKPARVGLGITTVLTMRTQW |
| 3. NK-K4C-M2GlyR p22 T19R S22W | KKKCPARVGLGITTVLTMRTQW |
| 4. NK4-M2GlyR p22 P5C T19R S22W | KKKKCARVGLGITTVLTMRTQW |
| 5. NK4-M2GlyR p22 A6C T19R S22W | KKKKPCRVGLGITTVLTMRTQW |
| 6. NK4-M2GlyR p22 V8C T19R S22W | KKKKPARCGLGITTVLTMRTQW |
| 7. NK4-M2GlyR p22 G9C T19R S22W | KKKKPARVCLGITTVLTMRTQW |
| 8. NK4-M2GlyR p22 L10C T19R S22W | KKKKPARVGCGITTVLTMRTQW |
| 9. NK4-M2GlyR p22 G11C T19R S22W | KKKKPARVGLCITTVLTMRTQW |
| 10. NK4-M2GlyR p22 112C T19R S22W | KKKKPARVGLGCTTVLTMRTQW |
| 11. NK4-M2GlyR p22 T13C T19R S22W | KKKKPARVGLGICTVLTMRTQW |
| 12. NK4-M2GlyR p22 T14C T19R S22W | KKKKPARVGLGITCVLTMRTQW |
| 13. NK4-M2GlyR p22 V15C T19R S22W | KKKKPARVGLGITTCLTMRTQW |
| 14. NK4-M2GlyR p22 L16C T19R S22W | KKKKPARVGLGITTVCTMRTQW |
| 15. NK4-M2GlyR p22 T17C T19R S22W | KKKKPARVGLGITTVLCMRTQW |
| 16. NK4-M2GlyR p22 M18C T19R S22W | KKKKPARVGLGITTVLTCRTQW |
| 17. NK4-M2GlyR p22 T19R T20C S22W | KKKKPARVGLGITTVLTMRCQW |
| 18. NK4-M2GlyR p22 T19R Q21C S22W | KKKKPARVGLGITTVLTMRTCW |

**Table 6**
Large unilamellar vesicles (LUVs) made by extrusion with POPC:POPE at different ratios (Error ± 1 nm). L/P ratio is 200/1.

| POPC (mol%) | POPE (mol%) | $\lambda_{max}$ (nm) |
|---|---|---|
| 0 | 0 | 355 |
| 100 | 0 | 355 |
| 90 | 10 | 348 |
| 80 | 20 | 349 |
| 70 | 30 | 346 |
| 60 | 40 | 345 |
| 50 | 50 | 348 |

ion conductances in epithelial monolayers suggested that the lack of complexity in composition of the synthetic membrane affect the insertion and assembly of the peptides. We therefore tested the ability and efficiency of insertion of NK$_4$-M2GlyR p22-T19R, S22W into liposomes composed of POPC: POPS, POPC:POPE and POPC:POPG (Tables 3–5). These experiments show maximal blue shifts of 21 and 10 nm measured when NK$_4$-M2GlyR p22-T19R, S22W was mixed with POPC:POPS and POPG (7:3) liposomes and a shift of 11 nm when mixed with POPC:POPE (6:4) liposomes, compared to dissolved peptide alone or liposomes alone with the absence of shifts. When the peptide was mixed with the vesicles composed of 100% POPC, which is a zwitterionic phospholipid, the peptide/liposome spectra did not give evidence of partition into the LUV (data not shown). One possible explanation is that the peptide may be lying on the surface of the liposome due to electrostatic interaction of the glycerol head groups on the phospholipids and oligo lysine N-terminus on the peptide.

The orientation of membrane proteins can be guided by a contact between negatively charged phospholipids and positively charged amino acid residues [54]. This is in agreement with results that show better insertion of peptide when it is exposed to phospholipid mixtures containing anionic phospholipids (POPC:POPS; 7:3), possibly due to more favorable attractive electrostatic interactions. Further when POPC:

POPS and POPC:POPE either at 10% or 20% of anionic phospholipid were tested results show that these ratios are insufficient to assist the peptide's insertion. Similarly 50% POPS or POPE also did not show an increase of blue shift indicating unfavorable conditions for peptide insertion.

## 4. Conclusions

Redesign of synthetic channel forming peptides based on the transmembrane segments of natural ion channel proteins is a challenging task. When assembling into a pore, NK$_4$-M2GlyR p22-T19R, S22W peptides form a synthetic construct resembling only the ion conductive part of its parent protein, therefore lacking a complex set of regulated control of assembly and function owned by its natural parent. However, lacking regulatory characteristics can be seen as limitations or a unique advantage. Various modifications of original putative protein sequences can lead to specific structure/function modified synthetic channels, carefully designed to meet the needs for targeted therapeutic use. The best candidate synthetic amphiphilic peptide, NK$_4$-M2GlyR p22-T19R, S22W presented in this study serves as a good scaffold for further detailed structure-function modifications aimed to tune its selectivity.

## Appendix A. Supplementary data

Supplementary data to this article can be found online at doi:10.1016/j.bbamem.2011.07.037.
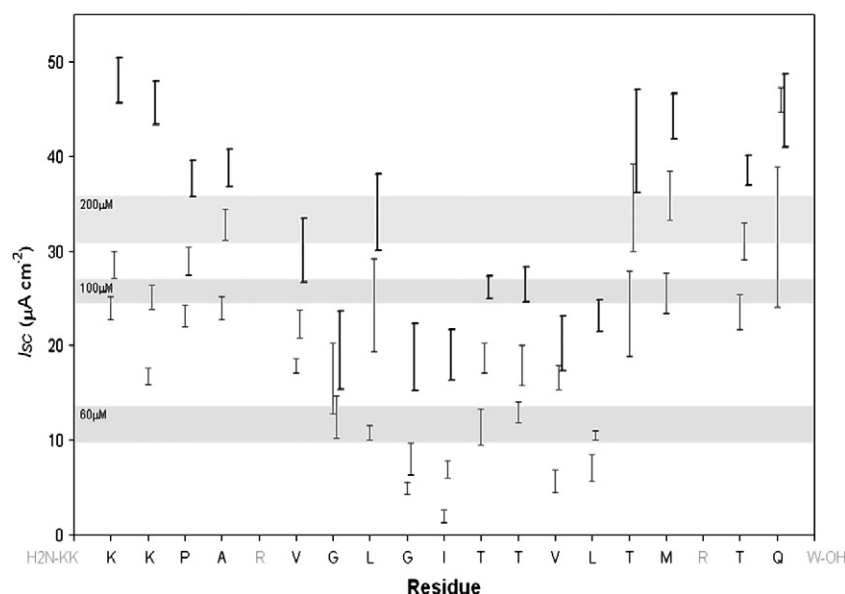


**Fig. 10.** Activities of cysteine substituted peptides applied to MDCK epithelial monolayers. The anion transport results for seventeen cysteine substituted peptides are shown. Short-circuit current ($I_{SC}$) data are shown at three peptide concentrations. Each vertical bar above a substituted residue represents the mean $I_{SC}$ ± s.e.m. and the relative thickness of the bar indicates the concentration (highest concentration has thickest line). The shaded horizontal regions indicate the mean $I_{SC}$ ± s.e.m. for the parent sequence NK$_4$-M2GlyR p22-T19R, S22W at 60, 100, and 200 μM concentrations. The offset vertical bars indicate $I_{SC}$ ± SEM values obtained for the same concentrations of the cysteine-substitutions for the amino acids shown at the bottom on the Figure.

# References

[1] M. Proesmans, F. Vermeulen, K. De Boeck, What's new in cystic fibrosis? From treating symptoms to correction of the basic defect, Eur. J. Pediatr. 167 (2008) 839–849.

[2] D.C. Gadsby, P. Vergani, L. Csanády, The ABC protein turned chloride channel whose failure causes cystic fibrosis, Nature 440 (2006) 477–483.

[3] P.M. Quinton, Physiological basis of cystic fibrosis: a historical perspective, Physiol. Rev. 79 (1999) S3–S22.

[4] R. Planells-Cases, T.J. Jentsch, Chloride channelopathies, Biochim. Biophys. Acta 1792 (2009) 173–189.

[5] M. Roselle Abraham, A. Jahangir, A.E. Alekseev, A. Terzic, Channelopathies of inwardly rectifying potassium channels, FASEB J. 13 (1999) 1901–1910.

[6] M. Benatar, Neurological potassium channelopathies, Q. J. Med. 93 (2000) 787–797.

[7] L. Gao, J.R. Broughman, T. Iwamoto, J.M. Tomich, C.J. Venglarik, H.J. Forman, Synthetic chloride channel restores glutathione secretion in cystic fibrosis airway epithelia, Am. J. Physiol. Lung Cell. Mol. Physiol. 281 (2001) L24–L30.

[8] F. Van Goor, S. Hadida, P.D.J. Grootenhuis, B. Burton, D. Cao, et al., Rescue of CF airway epithelial cell function in vitro by a CFTR potentiator, VX-770, Proc. Nat. Am. Sci. 10 (2009) 18825–18830.

[9] E. Abel, G.E.M. Maguire, E.S. Meadows, O. Murillo, T. Jin, G.W. Gokel, Planar bilayer conductance and fluorescence studies confirm the function and location of a synthetic, sodium-ion-conducting channel in a phospholipid bilayer membrane, J. Am. Chem. Soc. 119 (1997) 9061–9062.

[10] R. Pajewski, R. Garcia-Medina, S.L. Brody, W.M. Leevy, P.H. Schlesinger, G.W. Gokel, A synthetic, chloride-selective channel that alters chloride transport in epithelial cells, Chem. Commun. (Camb.) 21 (2006) 329–331.

[11] M.T. Tosteson, D.S. Auld, D.C. Tosteson, Voltage-gated channels formed in lipid bilayers y a positively charged segment of the Na-channel polypeptide, Proc. Natl. Acad. Sci. U. S. A. 86 (1989) 707–710.

[12] M. Montal, M.S. Montal, J.M. Tomich, Synporins-synthetic proteins that emulate the pore structure of biological ionic channels, Proc. Natl. Acad. Sci. U. S. A. 87 (1990) 6929–6933.

[13] S. Oiki, W. Danho, M. Montal, Channel protein engineering: synthetic 22-mer peptide from the primary structure of the voltage-sensitive sodium channel forms ionic channels in lipid bilayers, Proc. Natl. Acad. Sci. U. S. A. 85 (1988) 2393–2397.

[14] G.J. Kersh, J.M. Tomich, M. Montal, The M2δ transmembrane domain of the nicotinic cholinergic receptor forms ion channels in human erythrocyte membranes, Biochem. Biophys. Res. Comm. 162 (1989) 352–356.

[15] N. Le Novère, J.P. Changeux, LGICdb: the ligand-gated ion channel database, Nucleic Acid Res. 29 (2001) 294–295.

[16] M. Cascio, Structure and function of the glycine receptor and related nicotinicoid receptors, J. Biol. Chem. 279 (2004) 19383–19386.

[17] V. Schmieden, G. Grenningloh, P.R. Schofield, H. Betz, Functional expression in *Xenopus* oocytes of the strychnine binding 48 kd subunit of the glycine receptor, EMBO J. 8 (1989) 695–700.

[18] G.L. Reddy, T. Iwamoto, J.M. Tomich, M. Montal, Synthetic peptides and four-helix bundle proteins as model systems for the pore-forming structure of channel proteins. II. Transmembrane segment M2 of the brain glycine receptor is a plausible candidate for the pore-lining structure, J. Biol. Chem. 268 (1993) 14608–14615.

[19] D.P. Wallace, J.M. Tomich, T. Iwamoto, K. Henderson, J.J. Grantham, L.P. Sullivan, A synthetic peptide derived from glycine-gated Cl⁻ channel induces transepithelial Cl⁻ and fluid secretion, Am. J. Physiol. 272 (1997) C1672–C1679.

[20] M.O. Montal, L.K. Buhler, T. Iwamoto, J.M. Tomich, M. Montal, Synthetic peptides and four-helix bundle proteins as model systems for the pore-forming structure of channel proteins. I. Transmembrane segment M2 of the nicotinic cholinergic receptor channel is a key pore-lining structure, J. Biol. Chem. 268 (1993) 14601–14607.

[21] M.O. Montal, T. Iwamoto, J.M. Tomich, M. Montal, Design, synthesis and functional characterization of a pentameric channel protein that mimics the presumed pore structure of the nicotinic cholinergic receptor, FEBS Lett. 320 (1993) 261–266.

[22] M.O. Montal, G.L. Reddy, T. Iwamoto, J.M. Tomich, M. Montal, Identification of an ion channel-forming motif in the primary structure of CFTR, the cystic fibrosis chloride channel, Proc. Natl. Acad. Sci. U. S. A. 91 (1994) 1495–1499.

[23] T. Iwamoto, A. Grove, M. Oblatt-Montal, M. Montal, J.M. Tomich, Chemical synthesis and characterization of peptides and oligomeric proteins designed to form transmembrane ion channels, Int. J. Pept. Protein Res. 43 (1994) 597–607.

[24] J.M. Tomich, D. Wallace, K. Henderson, K.E. Mitchell, G. Radke, R. Brandt, C.A. Ambler, A.J. Scott, J. Grantham, L. Sullivan, T. Iwamoto, Aqueous solubilization of transmembrane peptide sequence with retention of membrane insertion and function, Biophys. J. 74 (1998) 256–267.

[25] M.R.R. de Planque, J.A.W. Kruijtzer, R.M.J. Liskamp, D. Marsh, D.V. Greathouse, R.E. Koeppe II, B. de Kruijff, J.A. Killian, Different membrane anchoring positions of tryptophan and lysine in synthetic transmembrane α-helical peptides, J. Biol. Chem. 274 (1999) 20839–20846.

[26] J.D. Faraldo-Gómez, B. Roux, Electrostatics of ion stabilization in a ClC chloride channel homologue from *Escherichia coli*, J. Mol. Biol. 339 (2004) 981–1000.

[27] J.R. Broughman, K.E. Mitchell, R.L. Sedlacek, T. Iwamoto, J.M. Tomich, B.D. Schultz, NH2-terminal modification of a channel-forming peptide increases capacity for epithelial anion secretion, Am. J. Physiol. 280 (2001) C451–C458.

[28] J.R. Broughman, L.P. Shank, W. Takeguchi, B.D. Schultz, T. Iwamoto, K.E. Mitchell, J.M. Tomich, Distinct structural elements that direct solution aggregation and membrane assembly in the channel-forming peptide M2GlyR, Biochemistry 41 (2002) 7350–7358.

[29] G.A. Cook, O. Prakash, K. Zhang, L.P. Shank, A. Robbins, Y.-X. Gong, T. Iwamoto, B.D. Schultz, J.M. Tomich, Activity and structural comparisons of solution associating and monomeric channel-forming peptides derived from the glycine receptor M2 segment, Biophys. J. 86 (2004) 1424–1435.

[30] L.P. Shank, J.R. Broughman, W. Takeguchi, G. Cook, A.S. Robbins, L. Hahn, G. Radke, T. Iwamoto, B.D. Schultz, J.M. Tomich, Redesigning channel-forming peptides: amino acid substitutions that enhance rates of supramolecular self-assembly and raise ion transport activity, Biophys. J. 90 (2006) 2138–2150.

[31] A.I. Herrera, A. Al-Rawi, G.A. Cook, J. Gao, T. Iwamoto, O. Prakash, J.M. Tomich, J. Chen, Structural characterization of the two pore-forming peptides: consequences of introducing a C-terminal tryptophan, Proteins 78 (2010) 2238–2250.

[32] S.H. White, G. von Heijne, Do protein-lipid interactions determine the recognition of transmembrane helices at the ER translocon? Biochem. Soc. Trans. 33 (2005) 1012–1015.

[33] F.W. van Ginkel, T. Iwamoto, B.D. Schultz, J.M. Tomich, Immunity of a self-derived, channel-forming peptide in respiratory tract, Clin. Vaccine Immunol. 15 (2008) 260–266.

[34] W. Meijberg, P.J. Booth, The activation energy for insertion of transmembrane alpha-helices is dependent on membrane composition, J. Mol. Biol. 319 (2002) 839–853.

[35] L.A. Carpino, G.Y. Han, The 9-fluorenylmethoxycarbonyl amino-protecting group, J. Org. Chem. 37 (1972) 3404–3409.

[36] G.B. Fields, R.L. Noble, Solid phase peptide synthesis utilizing 9-fluorenylmethoxycarbonyl amino acids, Int. J. Pept. Protein Res. 35 (1990) 161–214.

[37] I. Ivanov, X.L. Cheng, S.M. Sine, J.A. McCammon, Barriers to ion translocation in cationic and anionic receptors from the Cys-loop family, J. Am. Chem. Soc. 129 (2007) 8217–8224.

[38] F. Delaglio, S. Grzesick, G.W. Vuister, G. Zhu, J. Pfeifer, A. Bax, NMRPipe: a multidimensional spectral processing system based on UNIX pipes, J. Biomol. NMR 6 (1995) 277–293.

[39] T.D. Goddard, D.G. Kneller, SPARKY 3, University of California, San Francisco, 2004.

[40] S. Jo, Automated builder and database of protein/membrane complexes for molecular dynamics simulations, PLoS One 2 (2007) e880.

[41] S. Jo, T. Kim, V.G. Iyer, W. Im, Software news and updates-CHARNIM-GUI: a web-based graphical user interface for CHARMM, J. Comput. Chem. 29 (2008) 1859–1865.

[42] B.R. Brooks, R.E. Bruccoleri, B.D. Olafson, D.J. States, S. Swaminathan, M. Karplus, CHARMM: a program for macromolecular energy, minimization, and dynamics calculations, J. Comput. Chem. 4 (1983) (1983) 187–217.

[43] B.R. Brooks, C.L. Brooks III, A.D. Mackerell, L. Nilsson, et al., CHARMM: the biomolecular simulation program, J. Comput. Chem. 30 (2009) 1545–1615.

[44] J.P. Ryckaert, G. Ciccotti, H.J.C. Berendsen, Numerical-integration of cartesian equations of motion of a system with constraints — molecular-dynamics of N-alkanes, J. Comput. Phys. 23 (1977) 327–341.

[45] T. Darden, D. York, L. Pedersen, Particle Mesh Ewald-an N. Log(N) method for Ewald sums in large systems, J. Chem. Phys. 98 (1993) 10089–10092.

[46] J.C. Phillips, R. Braun, W. Wang, J. Gumbart, E. Tajkhorshid, E. Villa, C. Chipot, R.D. Skeel, L. Kal, K. Schulten, Scalable molecular dynamics with NAMD, J. Comput. Chem. 26 (2005) 1781–1802.

[47] W. Humphrey, A. Dalke, K. Schulten, VMD: visual molecular dynamics, J. Mol. Graph. 14 (1996) 33–38.

[48] O.S. Smart, J.G. Neduvelil, X. Wang, B.A. Wallace, M.S.P. Sansom, HOLE: a program for the analysis of the pore dimensions of ion channel structural models, J. Mol. Graph. Model. 14 (1996) 354–360.

[49] W.C. Wimley, S.H. White, Designing transmembrane alpha-helices that insert spontaneously, Biochemistry 39 (2000) 4432–4442.

[50] S.M. Sine, A.G. Engel, Recent advances in Cys-loop receptor structure and function, Nature 440 (2006) 448–455.

[51] R.J.C. Hilf, R. Dutzler, X-ray structure of a prokaryotic pentameric ligand-gated ion channel, Nature 452 (2008) 375–379.

[52] R.J.C. Hilf, R. Dutzler, Structure of a potentially open state of a proton-activated pentameric ligand-gated ion channel, Nature 457 (2009) 115–118.

[53] N. Bocquet, H. Nury, M. Baaden, C. Le Poupon, J.P. Changeux, M. Delarue, et al., X-ray structure of a pentameric ligand-gated ion channel in an apparently open conformation, Nature 457 (2009) 111–114.

[54] W. van Klompenburg, J. Nilsson, G. von Heijne, B. de Kruijff, Anionic phospholipids are determinants of membrane protein topology, EMBO J. 16 (1997) 4261–4266.